

Supplementary Information for

A Fractal Gripper: geometry adaptive manipulator with switchable mode

Jiaxin Huang *et al.*

This supplementary information file contains all supplementary materials.

This supplementary material includes:

Figs **S1** to **S8**

Tables **S1** to **S7**

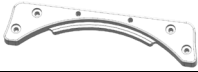
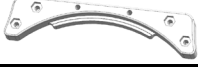






Equations **(S.1)** to **(S.6)**

Other supplementary material for this manuscript includes the following:

Movies **S1** to **S7**


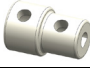
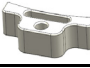



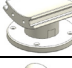
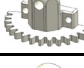

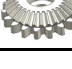

Data file **S1** to **S2**

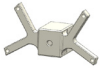

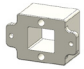




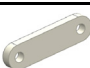
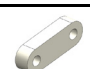
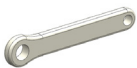

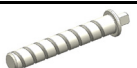




Table S1. Summary of 3D printing files for fractal structures.

File Name	Model Display*	Required Quantity
Top of the fractal rack.stl		1
Bottom of the fractal rack.stl		1
Fractal first piece top.stl		1
Fractal first piece bottom.stl		1
Fractal second piece top.stl		2
Fractal second piece bottom.stl		2
Fractal third piece top.stl		4
Fractal third piece bottom.stl		4

*Note: the scale of the Model Display is not to actual proportion.

Table S2. Summary of 3D printed files for gripper (without fractal structure).

File Name	Model Display*	Required Quantity
Axle drive bevel pinion.stl		2
Coupling.stl		1
Fixed pad.stl		1
Fixed support seat.stl		1
Fixed support seat_mirror image.stl		1
Flange fixing block.stl		1
Flange.stl		1
Floating gear seat.stl		4
Floating support seat.stl		6
Idler.stl		2
Movable rod.stl		2

Motor bracket fitting.stl		1
Motor bracket.stl		1
Motor cover fitting.stl		1
Motor cover plate.stl		1
Motor fixing plate.stl		2
Movable nut fitting.stl		1
Movable nut.stl		1
Movable rod fitting_1.stl		2
Movable rod fitting_2.stl		2
Oscillating rod.stl		2
Rocker.stl		3
Rotary screw.stl		1
Screw support.stl		1
Sleeve limit.stl		1
Sleeve limit_mirror image.stl		1
Support plate.stl		1

*Note: the scale of the Model Display is not to actual proportion.

Table S3. Summary of all parts for assembling fractal gripper.

Name of parts	Required Quantity	Materials
Fractal Structure	3	PLA
Gripper	1	PLA
Micro gear motor	1	metal
Biaxial microform motor	1	metal
Helical compression spring	numerous	stainless steel
Screw and nut	numerous	stainless steel

Table S4. The performance parameters of micro-gear motor.

Micro-gear motor	Screw drive	Mode-switching
Output shaft	Uniaxial	Biaxial
Reduction ratio	298	1030
Voltage (V)	12	12
No-load velocity (rpm)	60	16
Load velocity (rpm)	40	14
Rated torque (N·m)	0.176	0.097
Gridlock torque (N·m)	1.07	0.32

Table S5. The triangular pyramid volume in dual modes.

Triangular pyramid volume (cm ³)	Opening state	Closing state	Increased percentage
Grasping mode	134.76	2.65	98.03%
Gripping mode	147.51	6.99	95.26%

Table S6. Comparison of the advantages and disadvantages of the Fractal Gripper and the Fractal Vise.

Compare Object	Fractal Vise	Fractal Gripper
Force distribution	✓	✓
Self-recovery feature	✗	✓
Multi-scale adaptability	✓	✓
Switchable mode	✗	✓
Underactuated mechanism	✓	✓
Structural simplicity	✓	✗

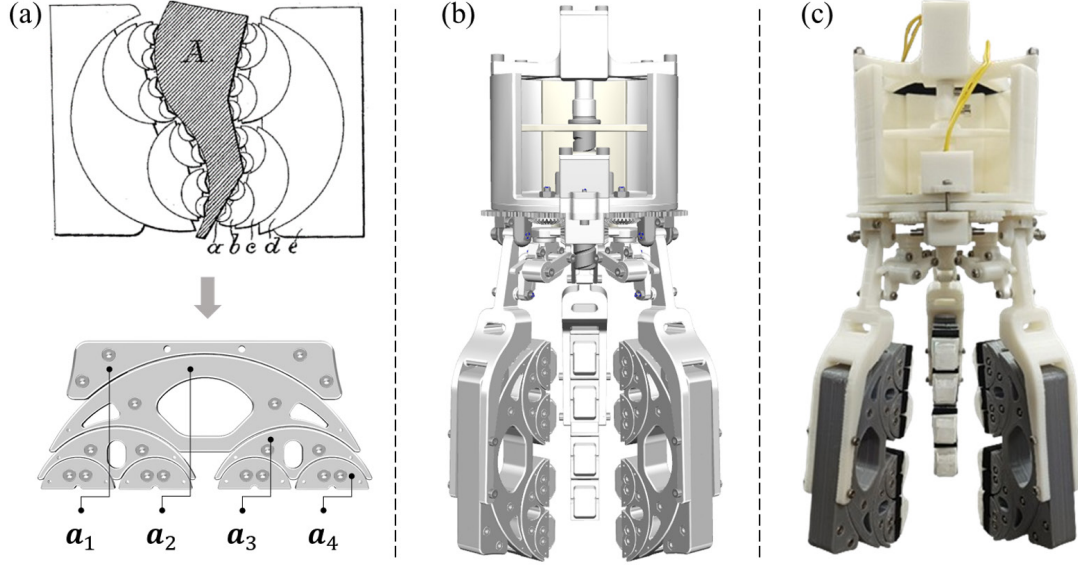


Fig. S1. Design inspiration of the fractal structure and physical prototype to the fractal gripper. (a) The design of the fractal structure is informed by Kunze's patent [51], and the components shown in the original patent include the fingers a , and the connecting layers b through e . These components work in concert to form a complex and robust structure for clamping and securing object A . In the fractal structure described in this work, there are four main parts: the fractal rack (a_1), the fractal first piece (a_2), the fractal second piece (a_3), and the fractal third piece (a_4). The connection between each part is achieved using T-slots. (b) Demonstrates model visualization of the 3D design of a fractal gripper. (c) Demonstrates the visualization of a fractal gripper from a 3D model to a physical object, with a scale size of 1:1. The 3D model file for the fractal gripper can be found in the **Data file S1**. All STL files (**Data file S2**) for the fractal gripper are shown in **Table S1** and **Table S2**.

The production details of the fractal gripper

To illustrate some of the fabrication details of the fractal gripper, a description is provided below in conjunction with **Fig. S2**. The names of the files constituting the fractal structure are listed in **Table S1**. The STL files for the fractal structure have been made available, allowing for reproduction through the 3D printing process. A demonstration of the slicing effect for the 3D printed file is presented in **Fig. S2**, where printing with a fill density of 90% or higher is recommended when using PLA or other plastic materials.

The flexible body is attached to the fractal third piece (a_4) within the fractal structure, with a description provided of the production process for fabricating the corresponding PDMS structure. First, a cavity container needs to be prepared; then, the PDMS liquid is poured into the container and cured with temperature; finally, the cured flexible body is obtained. In the liquid pouring step for PDMS, the main agent and curing agent must be mixed in a 1:1 ratio by weight or volume. After thorough mixing, the product's thickness should be observed for either atmospheric pressure or vacuum degassing. It is recommended that the curing temperature be increased to quickly shorten the curing time. However, for thicker products, caution is advised as too rapid curing may result in the formation of air bubbles.

During the assembly of the fractal gripper, it should be noted that some parts feature a half-and-half design. These parts (e.g., the floating gear seat) must be assembled to achieve a clearance fit with the circular bulge, allowing it to rotate circumferentially after assembly; otherwise, mode switching of the fractal gripper will not be feasible. For each part with a half-and-half design, through bores are reserved in the structure, which facilitates the use of screws and nuts for fixing.

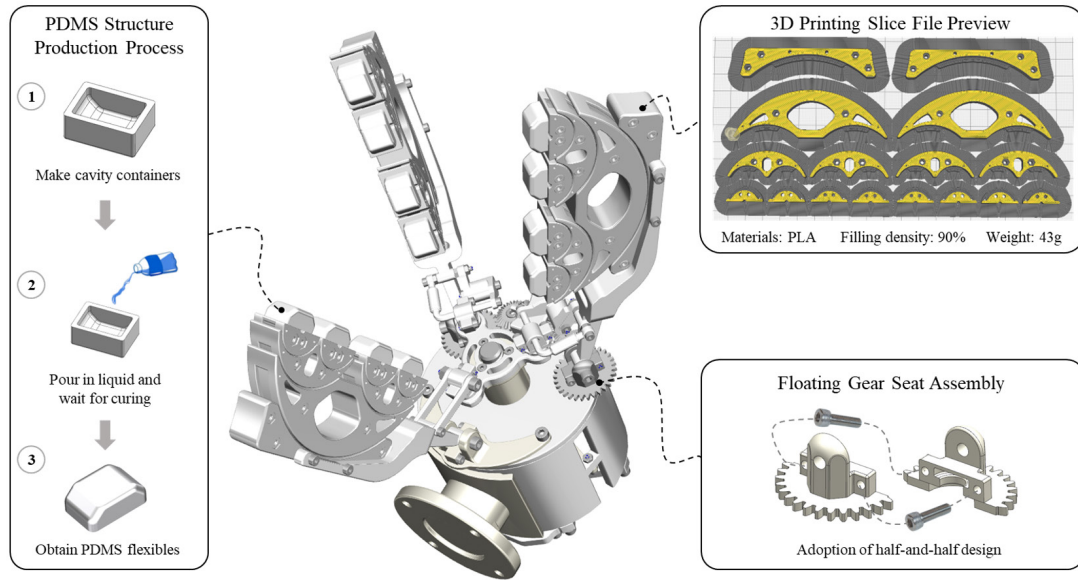


Fig. S2. Partial details regarding the fabrication and assembly of the fractal gripper are presented.

Grasping space and physical demonstration of the fractal gripper

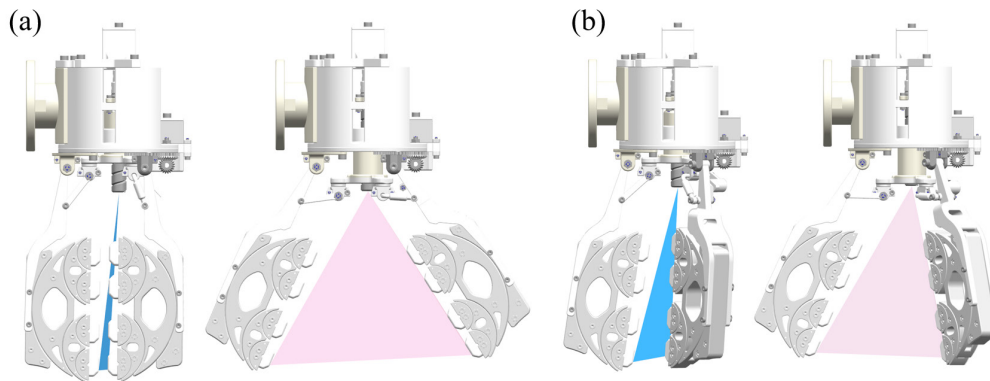


Fig. S3. The opening and closing bounds in dual modes. (a) Visualization of the triangular pyramid volume in gripping mode. (b) Visualization of the triangular pyramid volume in grasping mode.

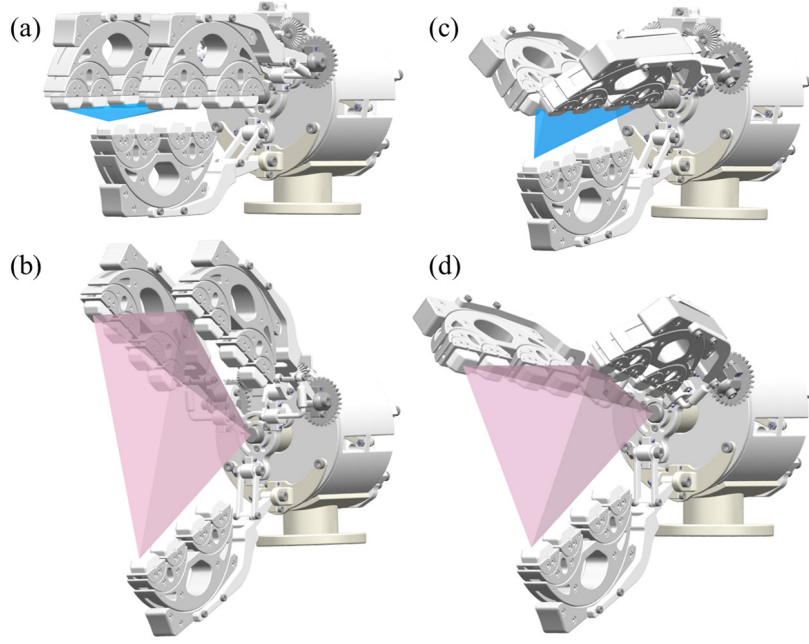


Fig. S4. Axonometric diagram of opening and closing bounds in dual modes. The blue and pink volume in the figure represent the visualization of the triangular pyramid volume. (a) represents the visualization of the triangular pyramid volume in the closing state of the gripping mode. (b) represents the visualization of the triangular pyramid volume in the opening state of the gripping mode. (c) represents the visualization of the triangular pyramid volume in the closing state of the grasping mode. (d) represents the visualization of the triangular pyramid volume in the opening state of the grasping mode.

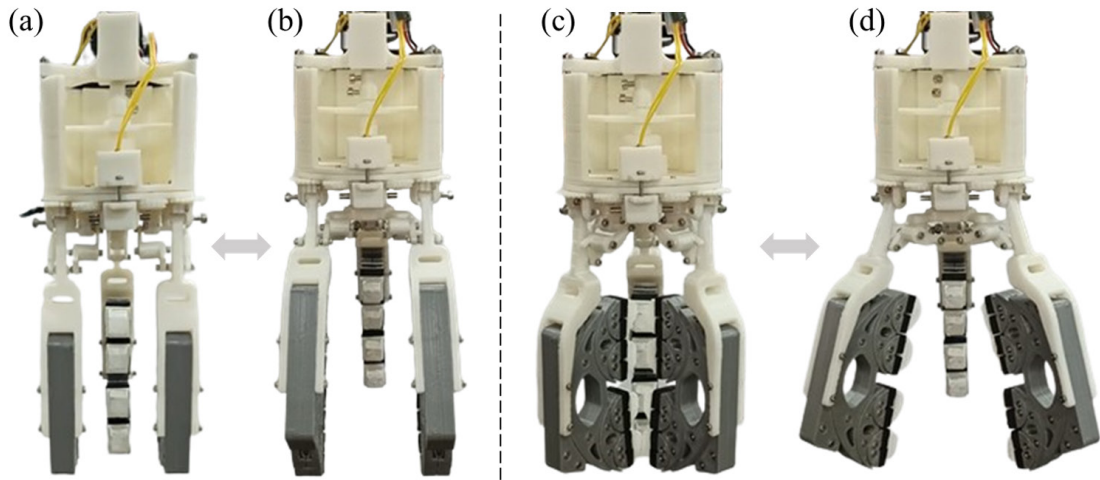


Fig. S5. The mode-switching, along with the opening and closing actions of the fractal gripper, is physically demonstrated. A related physics demonstration can be found in the attachment, **Movie S1**. ((a) and (b)) The gripping mode of the fractal gripper. ((c) and (d)) The grasping mode of the fractal gripper.

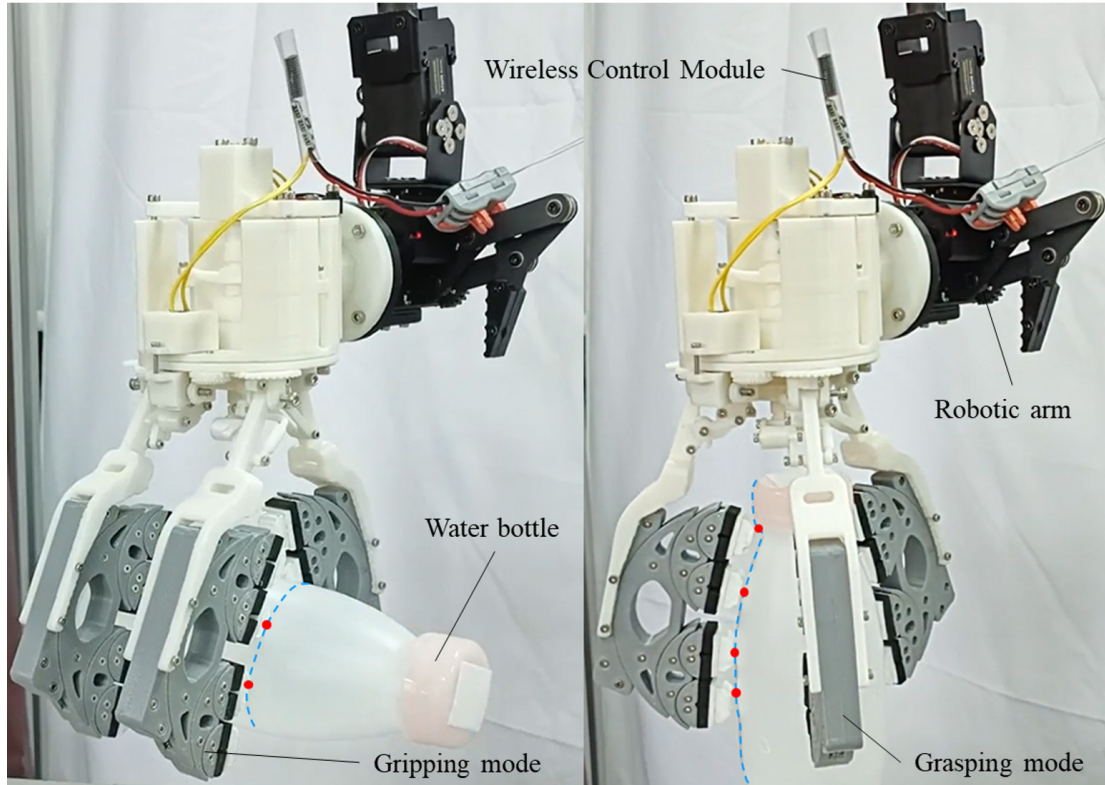


Fig. S6. Physical grab demo of a fractal gripper, analyzing a bottle as a case study. The fractal gripper is attached to the end position of the robotic arm by a flange. A demonstration was conducted to grasp the same bottle using different modes, and in combination with **Movie S3**, the fractal gripper's grasp stability was observed to be excellent. In the gripping mode, two flexible bodies in each fractal gripper come into contact with the surface of the bottle, resulting in a force distribution effect. In the grasping mode, four flexible bodies in each fractal gripper come into contact with the surface of the bottle, resulting in a more pronounced force distribution effect. In the figure, the contour of the bottle is depicted by the blue dotted line, while the red dot indicates the point of contact between the flexible body and the bottle's surface contour.

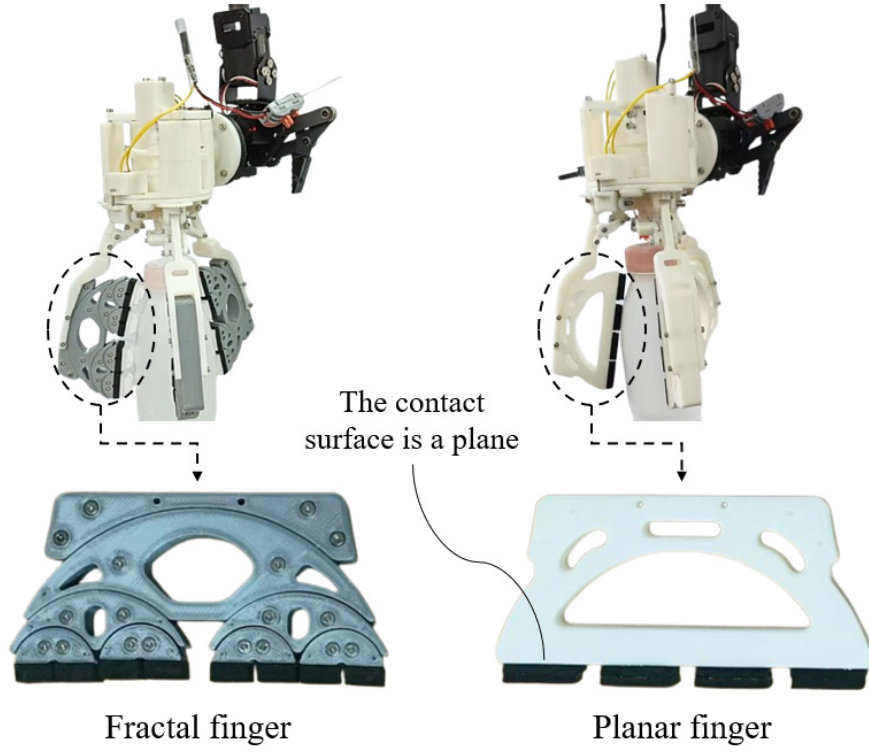


Fig. S7. Physical comparison of fractal finger and planar finger. The geometric design of the planar gripper is identical to that of the fractal gripper, but the contact surface is a plane.

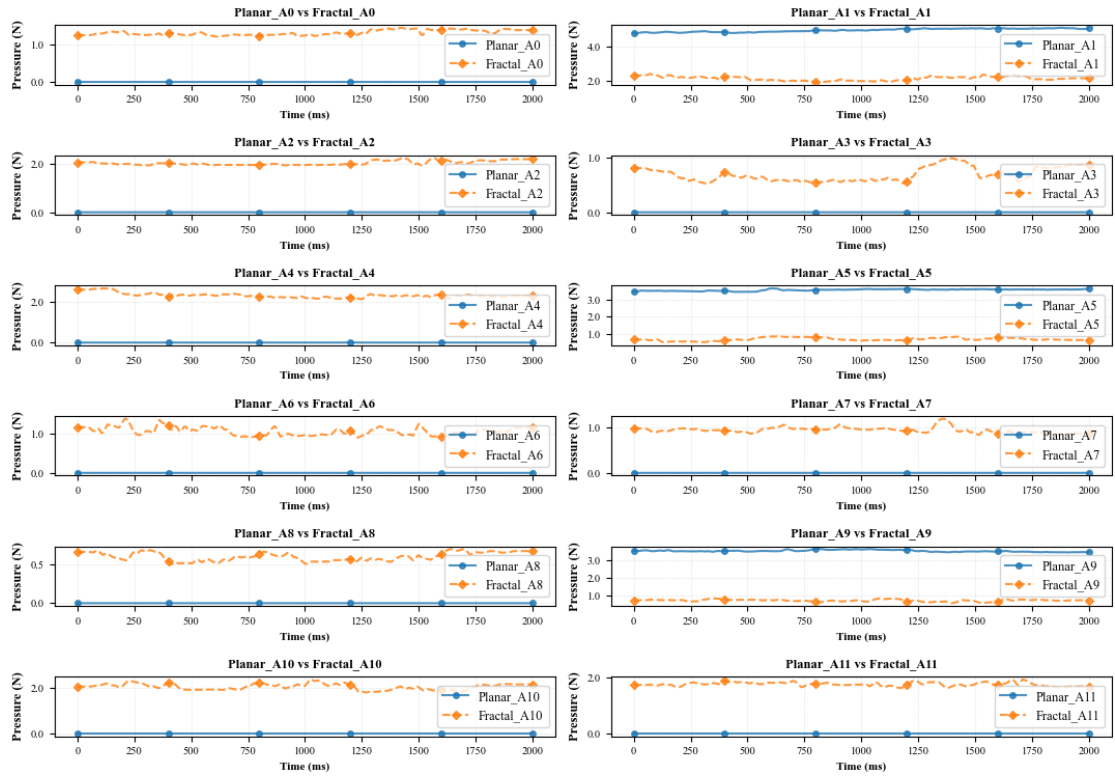


Fig. S8. The comparison of fingertip pressure curves between the Fractal and Planar grippers.

Table S7. Detailed comparison table of fingertip pressure data.

Planar / Fractal	Mean (N)	Std (N)	Max (N)	Min (N)
Planar_A0	0.00	0.00	0.00	0.00
Planar_A1	4.94	0.09	5.08	4.75
Planar_A2	0.00	0.00	0.00	0.00
Planar_A3	0.00	0.00	0.00	0.00
Planar_A4	0.00	0.00	0.00	0.00
Planar_A5	3.54	0.05	3.63	3.43
Planar_A6	0.00	0.00	0.00	0.00
Planar_A7	0.00	0.00	0.00	0.00
Planar_A8	0.00	0.00	0.00	0.00
Planar_A9	3.52	0.05	3.63	3.44
Planar_A10	0.00	0.00	0.00	0.00
Planar_A11	0.00	0.00	0.00	0.00
Fractal_A0	1.30	0.07	1.43	1.19
Fractal_A1	2.13	0.12	2.39	1.93
Fractal_A2	2.02	0.08	2.22	1.91
Fractal_A3	0.69	0.12	0.99	0.52
Fractal_A4	2.30	0.11	2.64	2.11
Fractal_A5	0.71	0.09	0.88	0.51
Fractal_A6	1.06	0.10	1.38	0.90
Fractal_A7	0.93	0.06	1.18	0.81
Fractal_A8	0.61	0.05	0.70	0.50
Fractal_A9	0.69	0.06	0.81	0.54
Fractal_A10	2.06	0.13	2.39	1.81
Fractal_A11	1.75	0.06	1.93	1.62

The fractal finger and fractal gripper Jacobian

The rigid body velocity of the k^{th} fingertip frame F_k in B_i , as per **Equation (5)**. Where $J_{F,i}(\eta_i)$ is the Jacobian matrix corresponding to the fractal finger. $\dot{\eta}_i$ is the vector of joint angular velocities. The specific form of the Jacobian matrix $J_{F,i}(\eta_i)$ is given in **Equation (S.1)**.

$$J_{F,i}(\eta_i) = \begin{bmatrix} \vec{\xi}_1 & \vec{\xi}_{2,1} & 0 & \vec{\xi}_{3,1} & 0 & 0 & 0 & \vec{\xi}_{4,1} & \dots \\ \vec{\xi}_1 & \vec{\xi}_{2,1} & 0 & \vec{\xi}_{3,1} & 0 & 0 & 0 & 0 & \dots \\ \vdots & \vdots & \vdots & \vdots & \vdots & \vdots & \vdots & \vdots & \dots \\ \vec{\xi}_1 & \vec{\xi}_{2,1} & 0 & 0 & \vec{\xi}_{3,2} & 0 & 0 & 0 & \dots \\ \vec{\xi}_1 & 0 & \vec{\xi}_{2,2} & 0 & 0 & \vec{\xi}_{3,3} & 0 & 0 & \dots \\ \vec{\xi}_1 & 0 & \vec{\xi}_{2,2} & 0 & 0 & \vec{\xi}_{3,3} & 0 & 0 & \dots \\ \vdots & \vdots & \vdots & \vdots & \vdots & \vdots & \vdots & \vdots & \dots \\ \vec{\xi}_1 & 0 & \vec{\xi}_{2,2} & 0 & 0 & 0 & 0 & 0 & \dots \end{bmatrix} \quad (\text{S.1})$$

Equilibrium grasp conditions of the fractal gripper

Each submatrix G_i ($i \in \{1, 2, 3\}$) represents the contact mapping for each finger. The grasp mapping matrix G_i for each finger is defined in **Equation (S.2)**.

$$G_i = \left[(Ad_{g_{OC_{i,1}^O}}^T, W_{i,1}), \dots, (Ad_{g_{OC_{i,2^{t-1}}^O}}^T, W_{i,2^{t-1}}) \right] \quad (\text{S.2})$$

The matrix $Ad_{g_{OC_{i,j}^O}}^T$ transforms the contact force matrix from the contact frame $C_{i,j}^O$ to the object frame O . This transformation is crucial for analyzing the dynamics between the fractal fingers and the object.

The lines of action of the contact force vectors $\vec{f}_{t,j}$ and $\vec{f}_{t,j+1}$ must pass through the axes of the joints to which their respective fingertips are connected. The magnitude and direction of the contact forces must satisfy the net zero-force equilibrium condition at the $(t-1)$ level parent joint, as per **Equation (S.3)**.

$$\tau_{t-1,j} = (f_{t,j} \cos(\eta_{t,j}) - f_{t,j+1} \cos(\eta_{t,j+1}))d_w^{t-1} / 2 - (f_{t,j} \sin(\eta_{t,j}) + f_{t,j+1} \sin(\eta_{t,j+1}))d_p^{t-1} = 0 \quad (\text{S.3})$$

Where, $\eta_{t,j}$ is the angle of the j^{th} fingertip link, where $j = 1, \dots, 2^{t-1}$.

If $\vec{f}_{i,j}$ represents the force passing through the axis of joint $J_{i,j}$, and all the child joints of $J_{i,j}$ satisfies the force equilibrium condition, then for levels 1 to $(t-1)$ of the joint tree, the following condition must be met as shown in **Equation (S.4)**.

$$\tau_{t-1,j} = (f_{t,j} \cos(\eta_{t,j}) - f_{t,j+1} \cos(\eta_{t,j+1}))d_w^{t-1} / 2 - (f_{t,j} \sin(\eta_{t,j}) + f_{t,j+1} \sin(\eta_{t,j+1}))d_p^{t-1} = 0 \quad (\text{S.4})$$

The torque balance conditions on the joints from levels 1 to $(t-1)$ provide $2^{t-1}-1$ scalar constraints on the 2^t-1 normal contact forces at the fingertips. If contact forces \vec{f}^{eq} satisfy the torque balance constraints, then for all $\alpha \in (0, \infty)$, $\alpha \vec{f}^{eq}$ also satisfies these constraints [55]. The direction of the reaction

force vector applied at the base joint J_1 depends on the equilibrium posture of the finger. The torque balance condition implies that its magnitude can be adjusted by a positive scalar factor α .

The set of all possible solutions to **Equation (12)** can be seen in **Equation (S.5)**.

$$\dot{\eta}_i = J_{F,i}^\dagger(\eta_{i,0})(\widetilde{W}_i^T T_{C_i C_i^o} T_{OC_i^o}^{-1} \dot{q}) + \dot{\eta}_{N,i} \quad (\text{S.5})$$

Where, $\dot{\eta}_{N,i}$ is any vector in the null space of $J_{F,i}(\eta_{i,0})$. $R(J_{F,i}^\dagger) = R(J_{F,i}^T)$, indicating that the Moore-Penrose pseudoinverse of the matrix $J_{F,i}$ has the same row space as its transpose. In equilibrium grasp, the matrix $J_{F,i}^T(\eta_{i,0})$ has a non-trivial null space, and the vector pointing towards the fingertip surface belongs to the null space of $N(J_{F,i}^T)$ [55]. The matrix \widetilde{W}_i^T projects the velocity $T_{C_i C_i^o} T_{OC_i^o}^{-1} \dot{q}$ onto the null space of $N(J_{F,i}^T)$ on the right-hand side of **Equation (S.5)**. Therefore, within $N(J_{F,i})$, only the internal joint movements $\dot{\eta}_{N,i}$ are possible solutions. These internal movements do not cause fingertip displacement.

This indicates that if the joint movements lie within the null space of the Jacobian matrix, these movements are internal adjustments that alter the joint positions without changing the actual position of the fingertips. Therefore, at a 1st-order analysis [55], when the object O is in equilibrium grasp, small perturbations in the object's position will not cause the fingertips to move along the contact normal.

Analysis of compliance effects and fingertip pressure

Equation (17) represents the total elastic energy of the three fingers under their respective stiffness matrices. See **Equation (S.6)** for the corresponding matrix equation.

$$PE = \dot{U}^T K \dot{U} \quad (\text{S.6})$$

This matrix form equation represents the potential energy PE as a quadratic form involving a series of stiffness matrices and velocity vectors. Where \dot{U} and K are respectively:

$$\dot{U} = \begin{bmatrix} \dot{u}_1 \\ \dot{u}_2 \\ \dot{u}_3 \end{bmatrix}, \quad K = \begin{bmatrix} K_1^1 + K_1^2 & 0 & 0 \\ 0 & K_2^1 + K_2^2 & 0 \\ 0 & 0 & K_3^1 + K_3^2 \end{bmatrix}$$